Modeling of metal thin film growth: Linking angstrom-scale molecular dynamics results to micron-scale film topographies

U. Hansen
Physik-Department and Walter Schottky Institute, Technische Universität München, D-85748 Garching, Germany and Department of Chemical Engineering, Massachusetts Institute of Technology, Cambridge, Massachusetts 02139

S. Rodgers and K. F. Jensen
Department of Chemical Engineering, Massachusetts Institute of Technology, Cambridge, Massachusetts 02139

(Received 17 September 1999)

A general method for modeling ionized physical vapor deposition is presented. As an example, the method is applied to growth of an aluminum film in the presence of an ionized argon flux. Molecular dynamics techniques are used to examine the surface adsorption, reflection, and sputter reactions taking place during ionized physical vapor deposition. We predict their relative probabilities and discuss their dependence on energy and incident angle. Subsequently, we combine the information obtained from molecular dynamics with a line of sight transport model in a two-dimensional feature, incorporating all effects of reemission and resputtering. This provides a complete growth rate model that allows inclusion of energy- and angular-dependent reaction rates. Finally, a level-set approach is used to describe the morphology of the growing film. We thus arrive at a computationally highly efficient and accurate scheme to model the growth of thin films. We demonstrate the capabilities of the model predicting the major differences on Al film topographies between conventional and ionized sputter deposition techniques studying thin film growth under ionized physical vapor deposition conditions with different Ar fluxes.

I. INTRODUCTION

The filling of contacts and vias is a well established technique for the advanced multilevel metalization, especially for sub-μm technology.[1] However, the shrinking of semiconductor device size to the sub-quarter-micron regime places stringent demands on metal deposition technology.[2] Sputter deposition, also known as physical vapor deposition, or PVD, is a widely used technique for depositing thin metal layers on semiconductor wafers. These layers are used as diffusion barriers, adhesion or seed layers, primary conductors, anti-reflection coatings, and etch stops,[3] and the reliability of thin films is crucial to die yield and device lifetime.[4] As semiconductor line-width dimensions have shrunk and the aspect ratios of vias and trenches have increased (aspect ratio = depth/width of a feature), it has become evident that conventional magnetron sputtering cannot meet future technology needs.[5] Currently aspect ratios for vias of 2:1 are common and ratios of 4:1 and 5:1 are expected in the near future.[6] In addition, the number of interconnected levels is increasing with the increased functional complexity and number of on chip transistors.[7]

Ionized physical vapor deposition (IPVD) has received much attention as a method for depositing material at the bottom and on the sidewalls of high aspect ratios proposed for sub-0.25-μm integration.[8] IPVD is based on in-flight ionization of atoms sputtered from a target. The metal atoms knocked out of the target by argon ions experience ionization as they pass through a high-density plasma generated by a radio-frequency antenna before reaching the substrate. The electric field at the biased substrate tends to collimate this metal ion flux.[9] From a practical point of view, IPVD has two intrinsic advantages over conventional sputtering. First, if the substrate is biased negatively, then positive ions will be accelerated toward the substrate causing incident metal ions arriving at near normal incidence. Second, the arriving energy of the metal depositing species is controlled by adjusting the bias voltage. IPVD improves the filling characteristics of the features by reducing the buildup of overhanging metal deposited at the mouth of the structure, and resputtering material from the feature bottom to the sidewalls.

Due to the growing technological demands for the sputter process an understanding of the underlying key processes at the atomic level is required.[10] Atomistic simulations are playing an increasingly prominent role in materials science, offering a microscopic physical view that cannot be readily obtained from experiment alone. Predictions resulting from this atomic level understanding are proving increasingly accurate and useful.[11] Hence there has been increased effort[12–16] to model highly nonthermal deposition techniques using the molecular dynamics (MD) approach.[17,18] The strengths of this technique are that it allows us to study atomic trajectories and thus to pursue the atomistics of the deposition. Using molecular dynamics data in growth modeling is an approach clearly superior to simplified continuum models, which usually do not include atomic level information at all and employ energy- and angular-independent rate constants.

In principle the reaction rates obtained from the MD or *ab initio* calculations can be employed in an atomistic cellular automaton or Monte Carlo (MC) model where the motion of each individual atom is traced during the course of the simulation.[16,19] Thus these approaches give insight into the atomistics of the deposition but they are computationally quite intensive, and consequently inconvenient if the final goal is to predict metal film topographies at length scales of

μm as opposed to Å. In many cases of practical interest, growth proceeds under simultaneous rare-gas bombardment, and the number of deposited particles and the number of particles etched away (resputtered) from the surface are of similar size. In such a case the overall growth rate is very low, but within atomistic MC, the trajectories of all atoms still have to be traced, making this approach too expensive to be useful for systems with very low growth rates.

In this paper we propose a computationally highly efficient scheme to model the growth of thin films. This approach enables us to employ data from atomistic simulations (i.e., angular- and energy-dependent surface reactions rates) within the level-set method.[20] Furthermore, all effects of reemissions are included so that we arrive at a model that provides a great speed advantage compared to the Monte Carlo methods while retaining the accuracy of an atomistic approach, and easily resolving problems with low growth rates.

The paper consists of three sections. The following section describes the modeling approach; we present molecular dynamics data for the Al system and describe how the molecular dynamics simulations are combined with a level-set profile advancement scheme. The following section includes an application of the model to the growth of Al under PVD and IPVD conditions. The final section contains a summary and conclusions.

II. MODELING APPROACH

In this work we begin by constructing a molecular dynamics based growth rate model, and combine it with a line of sight transport model within the feature. The resulting deposition model can account for arbitrary angular and energetic dependence of surface reaction rates and includes all effects of reemission and redeposition. Finally, a level-set scheme is combined with the reaction and transport model and is used to follow the film topography in time.

A. Reaction rates from molecular dynamics

We performed classical molecular dynamics simulations[17,18] using an embedded-atom-type[21,22] interaction potential for the Al-Al interaction and a repulsive Born-Mayer-type[23] term for the Ar-Al interaction. The details of the molecular dynamics calculations are described in previous work, see Refs. 16, 24, and 25. The incident Al atom is placed outside the interaction range of the surface. Its initial kinetic energy is set in the range of 0–150 eV and its starting angle off the surface normal in the range 0°–85°, which corresponds to typical ionized physical vapor deposition conditions. The trajectories of the incident atom, and of any other atom that may be etched away from the surface upon impact, are monitored. Analyzing a large number of trajectories per incident energy and angle, we collected a statistically significant sample (typically 200–1000 events) of well-defined adsorption, reflection, and etching events. The relative probability of the corresponding process is calculated as the ratio of the number of events of each kind to the total number. For the reflected particles and the particles sputtered away from the surface we also recorded the angular distributions after the impact. These distributions enter the function G (see Sec. II A 5). In the following we briefly discuss the energy and angular dependence of the three key surface reactions, namely, adsorption, reflection, and sputtering.

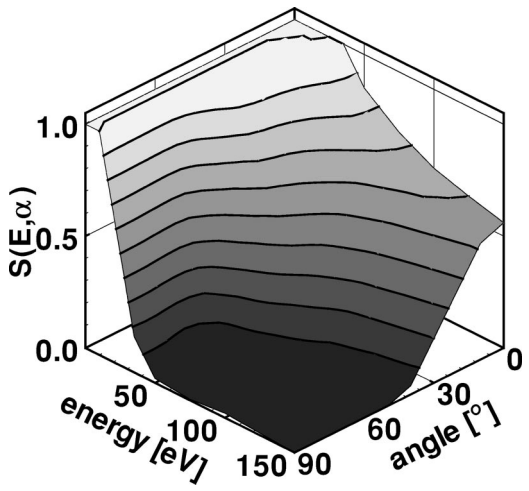

FIG. 1. Calculated sticking probabilities for hyperthermal Al atoms impinging on an Al(111) surface as a function of kinetic energy and incident off-normal angle α. The surface temperature was set to 450 K, i.e., about half the melting temperature and 20% above the Debye temperature. The contour lines mark increments of 0.1 in the sticking probability.

1. Adsorption of Al on Al(111)

In the low-energy regime (typical for molecular-beam epitaxy) all Al atoms are adsorbed independent of their impact angle. Since their initial kinetic energy is not sufficient to leave the strongly attractive surface adsorption well [the well depths are 3.10 eV on Al(111), 3.77 eV on Al(100), and 3.89 eV on Al(110) (Ref. 26)]. This picture changes if the incident kinetic energy is increased and a strongly energy- and angular-dependent sticking probability is found. The dependence of the sticking coefficient $S(E,\alpha)$ on the energy E and off-normal angle α for energies between 0 and 150 eV and incident angles in the range between 0° and 90° according to our MD calculations is depicted in Fig. 1. For high energies and large off-normal angles, particles are reflected so the adsorption probability drops to zero. In the intermediate angular range sputtering events (see Sec. II A 3) are the competing process that reduce the overall adsorption probability. From this figure is should be evident that using an angular- and energy-independent sticking probability is a very crude approximation for nonthermal deposition conditions.

2. Reflection of Al at Al(111)

We now turn our attention to the reflection events. With increasing angle we find a transition from diffuse to specular reflection events (for a detailed analysis see also Ref. 25). For large off-normal angles mainly the perpendicular momentum component is changed during the collision and the parallel component is conserved, such that the particle can escape the attractive adsorption well. This picture is reversed for the case of near-normal incidence. Very few reflections occur since the particle transfers most of its momentum to the surface. This is further confirmed by analyzing the parti-

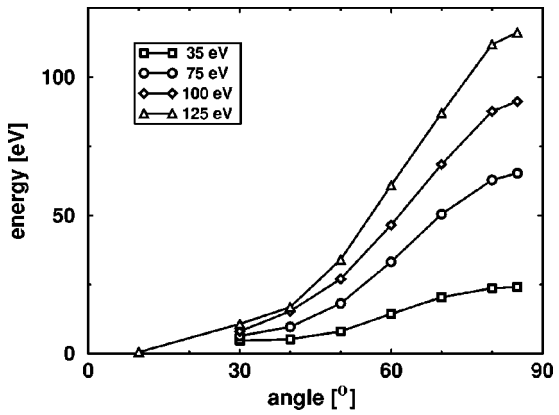

FIG. 2. Calculated mean kinetic energy for hyperthermal Al atoms being reflected from the Al(111) surface as a function of incident off-normal angle and energy. The open squares, circles, diamonds, and triangles correspond the energies of 35, 75, 100, and 125 eV, respectively. The surface temperature was set to 450 K, i.e., about half the melting temperature and 20% above than the Debye Temperature.

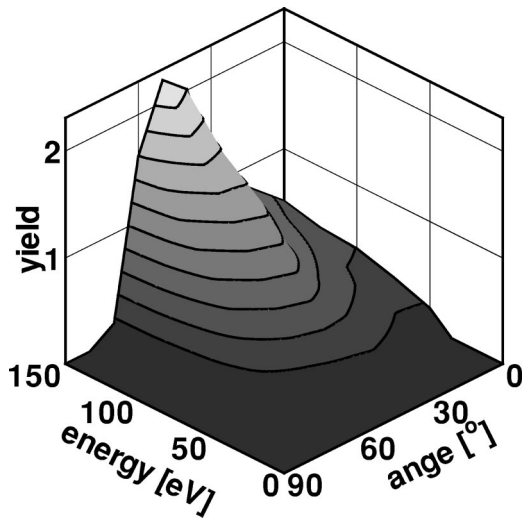

FIG. 3. Calculated sputter yield for hyperthermal Al atoms impinging on an Al(111) surface as a function of kinetic energy and incident off-normal angle α. The surface temperature was set to 450 K, i.e., about half the melting temperature and 20% above than the Debye temperature. The contour lines mark increments of 0.2 in the yield.

cle's kinetic energy after undergoing a reflection event. For a statistically significant sample we averaged the kinetic energy of particles being reflected from the surface. For incident energies in the range between 35 and 125 eV and off-normal angles between 10° and 85°, Fig. 2 shows the mean kinetic energy for particles being reflected from the surface.[27] The open squares, circles, diamonds, and triangles correspond the energies of 35, 75, 100, and 125 eV, respectively. For near-normal incidence the momentum transfer towards the surface is most efficient, while for near-grazing incidence the average energy loss is about 10 eV independent of the initial kinetic energy.

3. Sputtering of Al from Al(111)

Under nonthermal deposition conditions, the key physical processes are adsorption, reflection, and sputtering, i.e., the removal of surface atoms and adsorbates by the impact of energetic particles. During the sputter process not only single particles are etched away from the surface so that the yield, i.e., the number of particles leaving the surface divided by the number of particles impinging on the surface, is obtained by multiplying the sputter probability by the actual multiplicity for the event (multiplicity n means that upon impact of a single particle $n+1$ particles are sputtered from the surface). The yield for particles being etched away due to the impact of an energetic particle according to our MD calculations is shown in Fig. 3. Note that in contrast to the adsorption and reflection events, the etch yield does not show a monotone dependence on the parameters of incidence, i.e., energy and angle. More interestingly it reaches a maximum for angles around 50° and decreases as near-grazing angles are approached. For energies smaller than 25 eV no sputter events are observed. But increasing the energy we find considerable changes in the sputter yield. Even at small angle the etching probability and yield are nonvanishing. For small deviations from the normal incidence, the etch rate initially raises, since the probability of a surface atom to gain momentum directed away from the surface increases when the incident atom arrives at an oblique angle at the surface. At large off-normal angles the latter probability drops because of the competing specular reflection events. Analyzing the energies of the particles sputtered away from the surface we find, that they have mainly energies less than 15 eV such that they are most likely adsorbed in the course of their next interaction with the growing film front. Furthermore it should be pointed out that there is a preferred direction for the sputtered particles, which depends on the underlying crystal structure and surface orientation (see Ref. 25 for details).

4. Reaction rates for Ar on Al(111)

From experiments it is known that, if at all, a negligible fraction of Ar is incorporated into the film during growth. So as an excellent approximation we only have to consider the reflection and etching probabilities for Ar since basically no adsorption takes place. We find that for energies below 25 eV hardly any argon atom can etch away Al atoms from the surface. As in the case of Al the yield curves for Ar display a distinct maximum for off-normal angles around 45°.

5. Application of MD results to micron-scale thin film growth

As obvious from the previous discussion, there exists a complex balance between the different competing surface reactions. Only with an accurate description of their probabilities does reliable and predictive thin film growth modeling become feasible. Before the MD results can be used in a simulation of film morphology, they must be summarized in a fashion that is readily compatible with a species transport model. Given an incident vector flux, $\Phi^{in}(E^{in},\theta^{in})$, at a particular energy E^{in} and angle θ^{in}, a function $G_i(E^{in},\theta^{in}\rightarrow E^{out},\theta^{out})$ is used to relate the emitted and incident fluxes in a manner consistent with the pretabulated MD results for atoms of type i. Thus, $G_i(E,\theta\rightarrow E',\theta')$ summarizes all the surface events and gives the reemitted flux $\Phi^{out}(E',\theta')$ after operating on $\Phi^{in}(E,\theta)$. Operation of G for the data presented in the previous section is depicted in Fig. 4. In the top

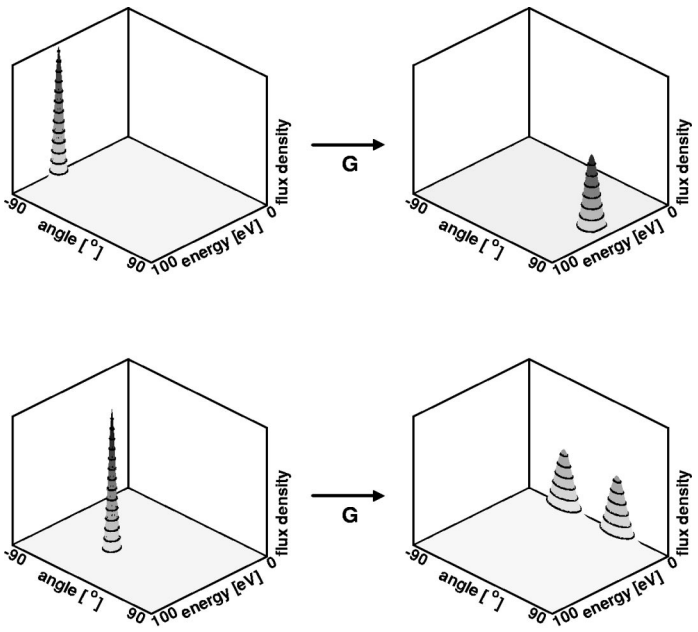

FIG. 4. Illustration of the effect of the function G that maps according to the sampled MD data an incoming vector flux density to the reemitted flux density. In the top left panel a narrow incident distribution impinging with a kinetic energy of 60 eV at an angle of $+85°$ is shown, the right panel depicts the corresponding reemitted distribution. The lower panels show the incoming and reemitted fluxes for an incident angle of 10° and an incident energy of 60 eV.

panel we show the effect of a narrow distribution impinging with a kinetic energy of 60 eV at an angle of $+85°$ (with respect to the surface normal) on the Al(111) surface. Under these conditions most of the incoming atoms are specularly reflected (see also Sec. II A 2) but lose on the average some of their initial kinetic energy such that the reflected distribution is broadened as can be seen in the right graph of the figure. If we decrease the initial angle to 10° (the lower panel in Fig. 4) most particles will etch away other particles form the surface such that the reemitted flux in this picture consists of two peaks centered around the preferential direction of reemitted particles (see Sec. II A 3). [Other examples of G: for a perfectly adsorbing process, i.e., the sticking coefficient is unity, $G_i(E,\theta\rightarrow E',\theta')=0$ holds, while for a perfect specular reflection with no energy loss $G_i(E,\theta\rightarrow E',\theta')=\delta(\theta+\theta')\delta(E-E')$.]

Once G_i is calculated for each energetic species i in the system, the reemitted flux $\Phi_i^{out}(\mathbf{r},E',\theta')$ can be determined for any given incident flux $\Phi_i^{in}(\mathbf{r},E,\theta)$ at a point $\mathbf{r}$, by Eq. (1) below,

$$\Phi_i^{out}(\mathbf{r},E',\theta')=\int_0^{\infty}\int_{-\pi/2}^{\pi/2} G_i(E,\theta\rightarrow E',\theta') \times\Phi_i^{in}(\mathbf{r},E,\theta)\,dE\,d\theta. \quad (1)$$

Here the integral runs over all the possible energies in the system $[0,\infty]$ and all the possible angles towards the surface normal $[-\pi/2,\pi/2]$.

Furthermore, note that a mass balance readily gives $v_i(\mathbf{r})$, the deposition (or etch) rate at $\mathbf{r}$ due to a particle of species i,

$$v_i(\mathbf{r})=\int_0^{\infty}\int_{-\pi/2}^{\pi/2}\Phi_i^{in}(\mathbf{r},E,\theta)\,dE\,d\theta - \int_0^{\infty}\int_{-\pi/2}^{\pi/2}\Phi_i^{out}(\mathbf{r},E',\theta')\,dE'\,d\theta'. \quad (2)$$

The first term accounts for the direct flux, the second term for the reemitted flux. The integrals again run over the possible angles and energies.

B. Iterative calculation of film growth rate

Once the atomic scale behavior of the system has been characterized, the next step is to examine transport of material to the feature and within the feature itself. In this work, gas phase collisions were neglected and transport is modeled as a line-of-sight process.

The neglect of collisions in the gas phase is appropriate at low pressures (typically 15–30 mTorr[3]) where the mean free path of the particles is of the order of several mm. In contrast the dimensions of the feature are typically μm. Thus, very few collisions would take place within the domain of the feature scale simulation.

Within the context of the feature scale model, material arriving from the reactor chamber is treated as arriving from a source just above the substrate surface. The flux from the source of each species, and its angular and energy distribution, are specified as inputs to the model.

After leaving the source the impinging particles can experience three possible surface reactions, namely, adsorption, sputtering, and reflection.

From an atomistic point of view, if a highly energized particle or ion hits the surface at a point $\mathbf{r}$ it will lose part of its kinetic energy and will, depending on its impact angle and the surface orientation, either be adsorbed, reflected, or will sputter away other surface atoms. Let us assume the particle is reflected. Then it can subsequently hit another piece of the surface $\mathbf{r}'$ and get either adsorbed or again reflected, etc. In such a scenario the point $\mathbf{r}'$ will act as an additional source. For a typical trench profile these two contributions are illustrated in Fig. 5. Panel (a) depicts for a point (1) at the sidewall the range of incident impact angles for the direct flux. The arrows show the directions of the source particles, the dark gray area marks the angular range of the source particles. In panel (b) the origin of the reemitted flux arriving at

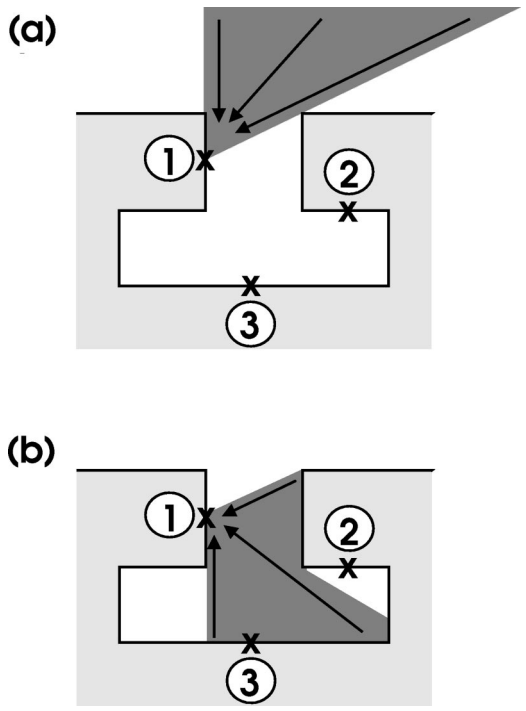

FIG. 5. Typical trench profile used in semiconductor processing. Points (1), (2) and (3) mark reference positions at the sidewall, the undercut, and at the bottom of the feature. Panel (a) depicts for point (1) the so-called direct flux, i.e., the flux from the source that can reach this point. Panel (b) illustrates the contribution from the re-emitted flux at (1), i.e., the particles that have been reflected or etched away after the initial impact. The arrows indicate the directions from where the material stems from. The dark shaded areas mark the angular range of the incoming flux.

(1) is shown. Now the flux is arriving from other points along the surface and the gray area marks those points, that can be ''seen'' by (1). Both contributions have to be considered for an accurate description of the front velocity at (1). We first focus on the contribution of the direct flux and then turn our attention to the reemitted flux. Thus, in every system with microscale topography, a nonunity sticking coefficient and/or a nonvanishing probability for resputtering implies that the total arriving flux stems from two possible reactions. The first one is the direct flux, i.e., the flux of atoms that leave the source and arrive at the surface before contacting another part of the feature. The second source of material is the flux due to reemissions, which stems from reflection and sputtering events. We term the contribution of the source as direct flux and the contributions due to reemissions as reemitted flux.

During IPVD growth in addition to metal atoms arriving from the source *S*, there will also be a significant flux of rare-gas ions, like Ar^+. The source *S* emits each species *i* with the angular- and energy-dependent vector flux density $\Phi_i^S(E,\alpha_S)$ where *E* is the energy of the released particle, α_S is the off-normal angle with respect to the normal of the source plane, and *i* is an index that describes the type of emitted particle (i.e., metal 1, metal 2, etc., rare-gas 1, rare-gas 2, etc.).

There is no restriction with respect to the angular and energy dependence of the source functions Φ_i^S and it will in general depend on the deposition conditions and on the details of the chamber. Φ_i^S can be either described by a simulation or input directly by the user. Furthermore it is assumed that the source does not change its emission characteristic on the length scale of the simulated domain.[28]

Knowing the fluxes from the source, the feature geometry, and *G* (see Sec. II A 5), the incident flux of each species *i* at any point **r**, on the feature surface can be written as

$$\Phi_i^{in}(\mathbf{r},E,\theta)=\Phi_i^S(E,g[\theta])+\Phi_i^{out}(\mathbf{r}',E,g[\theta]). \qquad (3)$$

The first term on the right represents the direct flux, the second represents the flux re-emitted from other points $\mathbf{r}'$ of the feature surface. The ray joining emitting points $\mathbf{r}'$ with receiving point **r**, makes angle θ with the receiving surface normal, and angle $g[\theta]$ with the normal of the emitting surface. An obvious difficulty with the equation above is that while Φ_i^S is known a priori, $\Phi_i^{out}(\mathbf{r}',E,g[\theta])$ is not. As mentioned previously, the adsorption rate, the sputter rate, and the reflection rate at a point **r** of the surface depend not only on the incoming vector flux densities, but also on the impact angle with respect to the local surface normal. The nature of these dependencies can be complex, and usually depends on the atomic structure of the growing film.[25] The implicit nature of the equation suggests an iterative approach, and the front velocity is thus obtained with the following scheme.

(1) Perform MD simulations to describe surface interactions for each important energetic species in the system.

(2) Calculate the flux arriving directly from the source for all points along the surface. Use the molecular dynamics results to determine the angular distribution and amount of reemitted flux (reflections and sputtering).

(3) For each point at the surface consider the reemitted fluxes from the other surface points; in addition, calculate the distribution of the flux that is again reemitted.

(4) Repeat points (1)–(3) as long as the reemitted flux is less than a small fraction of the initial flux, such that further iterations will not change the front velocity.

Thus during the first iteration the incoming flux is the flux due to the source $\Phi_i^S(E,g[\theta])$ and it holds:

$$\Phi_i^{in,(0)}(\mathbf{r},E,\theta)=\Phi_i^S(E,g[\theta]) \qquad (4)$$

and after the *n*th iteration,

$$\Phi_i^{in,(n+1)}(\mathbf{r},E,\theta)=\int_0^{\infty}\int_{-\pi/2}^{\pi/2} G_i(E',\theta'\rightarrow E,g[\theta]) \times\Phi_i^{in,(n)}(\mathbf{r}',E',\theta')\,dE'\,d\theta'. \qquad (5)$$

Hence the total incoming flux $\Phi_i^{in}(\mathbf{r},E,\theta)$ after the *n*th iteration amounts to

$$\Phi_i^{in}(\mathbf{r},E,\theta)=\Phi_i^S(E,g[\theta])+\sum_{k=1}^{n}\Phi_i^{in,(k)}(\mathbf{r},E,\theta). \qquad (6)$$

Within our numerical implementation of the equations above we discretize the integrals, and store the source and reemitted fluxes in matrices. This easily allows an angular resolution of 1° and a resolution in energy space of about 1

eV, such that we are constrained only by the available MD or experimental data. Overall we developed a highly efficient and accurate scheme.

We have so far omitted a discussion of surface diffusion, since we want to focus on the effects of the deposition and redeposition. Surface diffusion would yield an opposing effect to the buildup of cusps due to preferential sputtering at certain angles and hence would make the interpretation of the predicted thin film structures more difficult. In addition recent scanning electron microscope pictures show that for low T deposition the films have sharp cusps and corners[29] implying that under these conditions no long-range surface diffusion is present, or at least too slow to compete with the dominant processes of deposition and resputtering. It should be emphasized that the inclusion of curvature driven surface diffusion—the standard approach in continuum film growth models—according to the ideas developed by Mullins[30] is a straightforward task within the level-set formalism since curvature informations are naturally obtained.

C. The level-set method

The theoretical foundation for the level-set method was mainly developed by Sethian[31,20] and are briefly summarized here. Using the level-set approach, the shape of a moving boundary can be traced in time, given an initial shape and a speed $\mathbf{v}$ that determines how to move each point of the interface.

The level-set method avoids the shortcomings of other front tracking algorithms[33–35] and offers a highly robust and accurate state-of-the-art technique for tracking interfaces that works in any number of space dimensions.[32]

To be more specific, the level-set method describes the movement of a closed hyper-surface $\Gamma(t)$, that is, $\Gamma[0,\infty) \rightarrow R^N$, propagating with speed $\mathbf{v}$ in its normal direction, where $\mathbf{v}$ can be a function of various arguments including curvature, normal direction, etc. In the case of IPVD, the speed will be the local growth (or etch) rate. The main idea behind the level-set method is to embed this propagating interface as the zero level set of a higher dimensional function ψ. Let $\psi(x,t=0)$, where $x \in R^N$ is defined by

$$\psi(x,t=0) = \pm d, \tag{7}$$

where d is the distance from x to $\Gamma(t=0)$, and the plus (minus) sign is chosen if the point x is outside (inside) the initial hypersurface $\Gamma(t=0)$. For the evolution of ψ the following initial value partial differential equation can be obtained

$$\frac{\partial \psi}{\partial t} + \mathbf{v} \cdot \nabla \psi = 0, \tag{8}$$

$$\psi(x,t=0) = \pm d. \tag{9}$$

These equations are known as the level-set equations. Integration of the above equation yields the position of the moving front as a function of time.

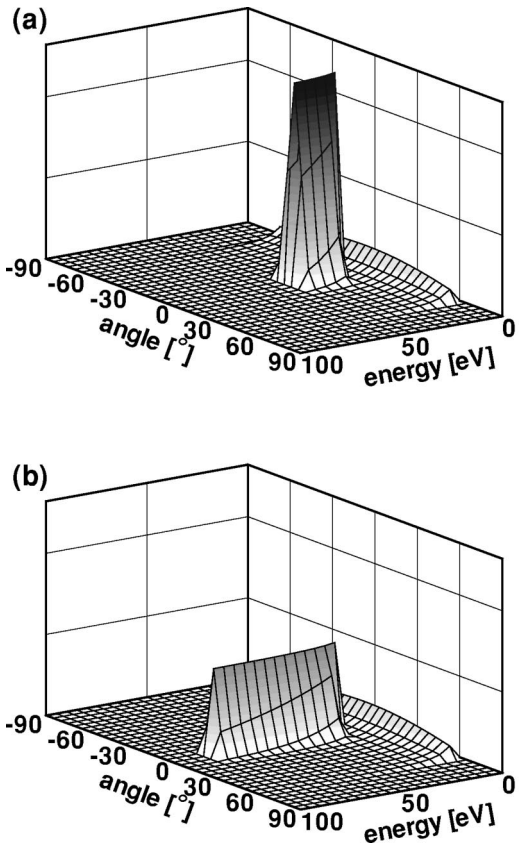

FIG. 6. Distribution of Al particles emitted from an IPVD source as a function of energy and off-normal angle. A self bias voltage of 20 V, an ionization of 80%, and a transverse temperature of 0.2 eV is assumed. Panel (a) depicts the source distribution function for a bias voltage of 40 V and in panel (b) the latter quantity is shown for a bias voltage of 80 eV.

III. APPLICATION TO Al THIN FILM GROWTH UNDER Ar ION BOMBARDMENT

In the following section we demonstrate the capabilities of our modeling approach and predict thin film topographies under various deposition conditions. We begin by choosing a source representative of typical IPVD conditions. Using the atomistic data obtained from MD calculations we are able to predict Al thin film growth without using adjustable parameters or semiempirical rules for the deposition.

A. Distribution function for the source

In this subsection we present an approximation for the energy and angular dependence of an IPVD source based on calculations by Kratzer *et al.*[36]

For conventional sputtering the energy and angular distribution are well described by a Thompson distribution[37] as experimentally confirmed.[38,39] For ionized physical vapor deposition this picture completely changes. Under IPVD conditions the metal atoms knocked out of the source by argon ions experience ionization as they pass through a high-density plasma generated by a radio-frequency antenna before reaching the substrate. The electric field at the biased substrate collimates and accelerates the ions. The normal velocity of the ions (metal and rare gas) can be approximated by a constant distribution that starts at the so-called self-bias

U_{SB} and extends to the applied bias voltage U_B.[36] The transversal component of the velocity is well described by a Maxwellian distribution with a temperature typically equal to $0.1-0.3$ eV. Recent experimental studies[40] on the deposition of Ti revealed transverse temperatures in the range between 0.13 and 0.18 eV. A large fraction, 80%, of the metal atoms is ionized and is described within the model outlined above; the remaining 20% neutrals are assumed to follow the Thompson distribution. For the total distribution we superpose the latter contributions. Figure 6 shows for 80% ionization, a self-bias voltage of 20 eV, and a transverse temperature of 0.2 eV, the energy and angular dependence of the model source function. In panel (a) a bias voltage of 40 V is applied and in panel (b) a bias voltage of 80 V is applied. In both cases there exist two characteristic regimes: the low-energy regime ($\leqslant 15$ eV), which displays a broad angular distribution due to the neutral atoms and is peaked at low energies ($\simeq 3$ eV), but has a long tail towards higher energies, and the high-energy regime, which is due to the ionized atoms and has in contrast a much narrower angular width. For the larger bias voltage [panel (b)] the range of energies extends to higher values and due to the normalization the corresponding peak is less pronounced than in the case of the lower bias voltage.

As the mass of Ar and Al is very similar their ion distributions are not very different[36] and one can take the same distributions for both species. Since only ionized argon with a high kinetic energy can etch away Al atoms of the film front or suffer a reflection, thermal Ar atoms will not influence the film growth and are not included in our model.

B. Example of Al thin film growth

In the following section we illustrate the importance of using angular and energy-resolved surface reaction probabilities in thin film growth modeling. Next we discuss the major differences in the film topographies for conventional and ionized sputter deposition and the last section describes the effect of Ar ion bombardment on the growing film front.

1. Effect of reemission and spectral resolved reaction probabilities

To gain a better understanding of the importance of the different fluxes (direct and reemitted) we discuss their contribution for a structure representative of those encountered in semiconductor manufacturing. Figure 5 shows a side view of this structure and (1) and (3) mark points at the sidewall and at the bottom, respectively. In the following we restrict the discussion for simplicity to the deposition of Al (without the rare-gas Ar), which is emitted according to the distributions described in Sec. III A. We assume a self-bias voltage of 20 V, an ionization fraction of 80%, an applied bias voltage of 80 V, and a transverse temperature of 0.2 eV. Due to geometrical limitations and the narrow angular distribution of the ionized flux of the source all particles from the source that reach the bottom of the feature, i.e., point (3), will impinge near normal at the surface. According to our molecular dynamics based reaction rates these particles will either be adsorbed or they will sputter other Al atoms away from the surface. There will be hardly any reflection events. Consequently the major contribution to the reemitted flux will be due to etching events. Panel (a) of Fig. 7 shows as a function of energy and off-normal angle the distribution of flux that is reemitted from point (3). There are two peaks centered around $\pm 35°$, the preferred direction for reemitted particles leaving the surface.[25] Although the source emits a wide range of energies (see Fig. 6) most of the particles leaving the surface at (3) have a rather low energy. Due to the wider angular distribution of the nonionized fraction of the Al atoms these atoms are preferentially adsorbed at the top or sidewalls of the structure such that they do not significantly contribute to the reemitted flux at (3). The reemitted flux at the sidewall of a feature [point (1) in Fig. 5] is quite different. The ionized contribution to the incoming flux hits the sidewall at near glazing angles. Thus reflections will be the dominant process at this point. In addition a small fraction of the nonionized particles can participate in etching events. Panel (b) shows the reemitted flux for point (1) at the sidewall. As can be seen the dominant contribution is peaked at rather large off-normal angles and extending to rather high energies. Thus, the flux of metal shows both significant quantitative and qualitative (in terms of incident angles and energetics) variation over the surface of the feature. The next section will demonstrate how these differences in flux influence the final conformality of the deposited film. In this case, notice that reemissions from the sidewall will lead to an en-

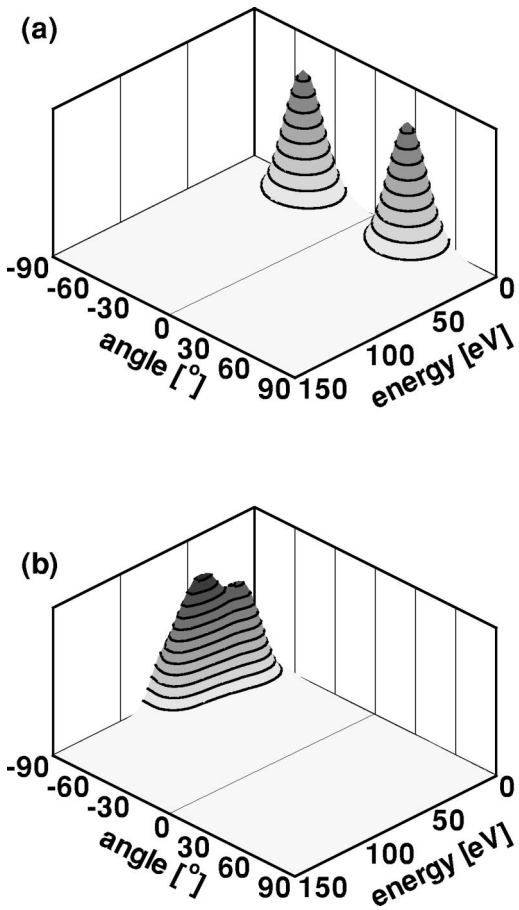

FIG. 7. Reemitted flux as a function of energy and off-normal angle for the bottom [panel (a)] and the sidewall [panel (b)] of a trench structure according to molecular dynamics reaction rates. The depicted fluxes correspond to points (1) and (3) in Fig. 1, respectively.

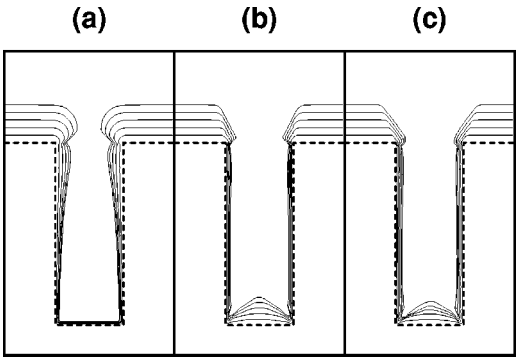

FIG. 8. Simulated thin film topographies under different deposition conditions for a trench structure with an aspect ratio of 3:1 and a width of 0.2 μm. In panel (a) an Al film under PVD conditions is deposited where the source function is described by the Thompson distribution. In (b) part of the incoming Al flux (80%) is ionized and modeled by a highly collimated angular distribution and finally in (c) the same deposition conditions as in (b) are applied with an additional flux of Ar.

hanced filling of the bottom of the feature and reemission from the bottom will bring material to portions of the trench that cannot be reached directly by the source, e.g., point (2) in Fig. 5 (see also Secs. III B 2 and Sec. III B 3).

2. Comparison of PVD and IPVD growth

We first take a closer look at the differences of the thin film properties under conventional magnetron sputtering conditions and ionized physical vapor deposition. For PVD deposition—as discussed earlier (see Sec. III A)—the distribution of the arriving particles is described by a Thompson distribution.[37] Due to the geometry of a deposition chamber the angular distribution does not extend to angles up to $\pm 90°$, but will be limited by typically $\pm 60°$ as suggested by Hamaguchi and Rossnagel.[29] Since for the PVD case most of the atoms have a rather low energy we do not expect a significant contribution to the speed function due to reflection and sputtering events. Only the atoms in the high-energy tail of the distribution carry enough kinetic energy not to be adsorbed upon their initial impact. For simplicity, we restrict our predictions to the deposition of Al neglecting the effect of Ar. Panels (a) of Fig. 8 and Fig. 9 show the resulting thin film topographies deposited on a trench with an aspect ratio of 3:1 and a width of 0.2 μm and an undercut structure with an opening of 0.2 μm and a width of the undercut of 0.4 μm. In both figures the solid contour lines show for constant time intervals the evolving film front, the dashed lines depict the initial geometry before the metal deposition. Due to the relatively wide distribution in angular space only a few particles can reach the bottom of the trench and undercut the structure. Most particles are adsorbed when they hit the trench sidewall thus leading to a buildup of material at the opening. This buildup of material further shadows the bottom regions such that in the course of the deposition less material can make its way to the bottom. As a consequence of the broad angular distribution in the PVD case there is a pileup of deposited metal at the bottom of the undercut structure that vanishes towards the corners due to geometrical shadowing. Another characteristic is that there is no deposition right below the accumulated material. This is due to the source not emitting at large off-normal angles and no material can reach this portion of the film. Hence there are cusps in the film right below the opening of the trench. For high aspect ratios the buildup of material at the opening of the trench will finally cause a closure at the top of the structure and a void in the metal film will persist. The hole in the metal film enhances electromigration in the finished device that adversely affects the reliability of such a structure.

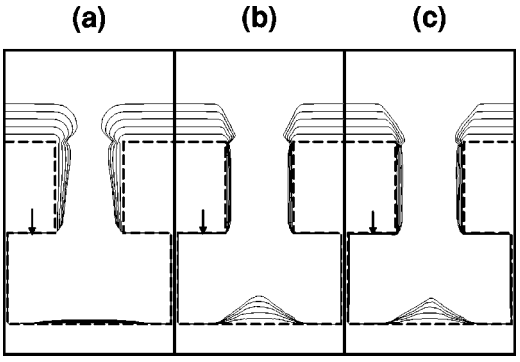

FIG. 9. Simulated thin film topographies under different deposition conditions for an undercut structure with a width of 0.2 μm at the opening and 0.4 μm at the undercut. In panel (a) an Al film under PVD conditions is deposited where the source function is described by the Thompson distribution. In (b) part of the incoming Al flux (80%) is ionized and modeled by a highly collimated angular distribution and finally in (c) the same deposition conditions as in (b) are applied with an additional flux of Ar. The arrows mark positions geometrically shadowed from the source. The film thicknesses at these points amount to ~ 0 Å, ~ 20 Å, and ~ 50 Å for (a), (b), and (c).

Next we will discuss the effect of the ionized atoms in IPVD deposition. For an IPVD source with a emission distribution as depicted in Fig. 6(b) we show the film fronts at different stages of growth in Fig. 8(b) and Fig. 9(b), respectively. Here Al thin film growth is considered neglecting the effects of Ar (the effect of Ar is discussed in Sec. III B 3). As in panels (a) of Fig. 8 and Fig. 9 the solid contour lines show for constant time intervals the evolving film front; the dashed lines depict the initial geometry before the metal deposition. To make a qualitative comparison between the different deposition conditions the front velocity was scaled such for the PVD and IPVD case [panels (a) and (b), respectively] the growth rates on the flat surface were equal. Comparing panels (a) and (b) there are two major differences between the different deposition conditions: first, the increased bottom and sidewall coverage for the IPVD source and second the appearance of bevel film front at the opening of the trench structure. Due to the collimation of the impinging atoms there is nearly as much material deposited at the bottom of the trench as on the flat surface. For the undercut structure the collimation leads to an enhanced pileup of material at the center part of the feature. An improvement in sidewall coverage and deposition at parts of the undercut structure that are geometrically shadowed from the source is obtained as material is resputtered from the large deposit at feature bottom. The pileup of material at the bottom is beveled towards the edges due to the maximum in the etch rate at angles around 45° (see Fig. 3). This maximum in the etch rates also leads to the development of the corner at the opening of the

trench structure. Since in the PVD case the energy of most of the impinging metal atoms is too low to etch away surface atoms during impact there is no effect of beveling and the film at the opening of the trench has a smooth shape.

The above discussion clearly shows the advantages of the IPVD deposition compared to the PVD deposition. In the following we will address the effect of the Ar atoms.

3. IPVD deposition under different Ar fluxes

In this subsection we investigate the effect of the Ar ions during metal thin film growth. As discussed in Sec. III A the Ar and Al atoms have approximately the same distribution at the source. The ratio of Ar to Al flux depends strongly on the deposition conditions and is unknown for most systems. In the following we will address the effect of the additional Ar on the film topographies and perform simulations for Al deposition with simultaneous Ar bombardment. Ar influences the growing film by sputtering deposited Al atoms from the surface. With this in mind, we expect that the Ar atoms will further reduce the buildup of overhangs at the opening of the structure. In addition, energetic Ar will also sputter material at the bottom of the feature, reducing the ''pile up'' at the bottom of the trench. The material sputtered from the bottom of the trench will reach the sidewall and increase the film thickness there.

In order to further investigate the impact of the Ar ions on the resulting film structures we performed simulations for an Al/Ar ratio of 1:1. Using the same deposition conditions as for the Al IPVD deposition described in Sec. III B 2 and again scaling the front velocity to the same value as in (a) and (b) at the flat portions of the surface. We show the resulting thin film topographies in panels (c) of Fig. 8 and Fig. 9. It is evident that the additional Ar bombardment according to the discussion above improves the sidewall coverage, and enhances deposition at the shadowed parts of the undercut structure. For the undercut structure the film thickness at the point marked by the arrows [or position (2) in Fig. 5] is more than doubled from $\sim$20 Å in the IPVD case without Ar to $\sim$50 Å in the presence of Ar. Furthermore Ar sputtering reduces the pileup of material at the bottom of the trench and reduces the buildup of overhangs at the opening of the trench. Thus the overall film is more conformal compared to the IPVD deposition without Ar and hence comes closer to the properties the microelectronic industry desires. We propose that the adjustment of the Ar flux is a promising way to achieve highly conformal metal thin films, if acceptable deposition rates could be maintained.

IV. SUMMARY

We have presented a general approach to implement angular- and energy-dependent surface reaction rates within the level-set formalism. We begin by presenting molecular dynamics data for hyperthermal Al and Ar atoms interacting with Al surfaces and discuss the energy and angular dependence of the three major surface reactions, namely, adsorption, reflection, and sputtering.

We summarize the surface interactions in a function G that calculates the flux returning from the surface for a given incident flux. Using the MD data in this fashion, we construct a general growth rate model and examine Al thin film growth under various deposition conditions.

We describe in detail an iterative method to calculate the speed function and point out the importance of the different flux contributions (direct and reemitted). Finally, the information is passed to a level-set description of the evolving film. The resulting simulator thus allows atomic scale MD information to be directly incorporated in a micron scale description of the evolving thin film. This approach is much faster than an atomistic Monte Carlo model, particularly when rare gases are included in the simulation.

Our calculations capture the major differences between IPVD and PVD deposition and display the strengths of deposition with high-energy ions, namely, a more conformal sidewall coverage and a better bottom coverage. Different levels of Ar ion fluxes have been compared; the additional sputtering of Ar further reduces the buildup of material at the opening of the trench structure and enhances the conformality in overall film thickness. We propose that the Ar flux can be a useful tuning parameter in microelectronics processing. By coupling this model with an equipment model, a complete IPVD process optimization could be performed.

ACKNOWLEDGMENTS

We thank Professor Dr. P. Vogl for helpful discussions and valuable guidance throughout the project. U.H. gratefully acknowledges financial support by the Infineon AG and the Deutsche Forschungs-Gemeinschaft under Contract No. DFG-SFB 348. S.R. thanks the SRC for funding under Contract No. 704.002.

[1] H. J. Barth, in *Polycrystalline Thin Films—Structure, Texture, Properties, and Applications*, edited by S. M. Yalisove *et al.*, MRS Symposia Proceedings No. 472 (Materials Research Society, Pittsburgh, 1997), p. 253.

[2] W. Wang, J. Foster, T. Snodgrass, A. E. Wendt, and J. H. Booske, J. Appl. Phys. **85**, 7556 (1996).

[3] S. M. Rossnagel, IBM J. Res. Dev. **43**, 163 (1999).

[4] M. K. Sheergar, T. D. Smy, S. K. Dew, and M. J. Brett, J. Vac. Sci. Technol. B **14**, 2595 (1996).

[5] S. M. Rossnagel and J. Hopwood, Appl. Phys. Lett. **63**, 3285 (1994).

[6] S. S. Winterton, T. Smy, S. K. Dew, and M. J. Brett, J. Appl. Phys. **78**, 3572 (1995).

[7] C. Whitman, M. M. Moslehi, A. Paranjpe, L. Velo, and. T. Omstead, J. Vac. Sci. Technol. A **17**, 1993 (1999).

[8] F. Cerio, J. Drewery, E. Huang, and G. Reynolds, J. Vac. Sci. Technol. A **16**, 1863 (1999).

[9] Z. C. Lum, J. E. Forster, T. G. Snodgrass, J. H. Booske, and A. E. Wendt, J. Vac. Sci. Technol. A **17**, 840 (1999).

[10] J. Dabrowski, H.-J. Müssig, M. Duane, S. T. Dunham, R. Goossens, and H.-H. Vuong, Adv. Solid State Phys. **38**, 595 (1998).

[11] A. F. Voter, MRS Bull. **21**, 17 (1996).

[12] X. W. Zhoua and H. N. G. Wadley, Surf. Sci. **431**, 42 (1999).

[13] D. E. Hanson, A. F. Voter, and J. D. Kress, J. Appl. Phys. **82**,

3552 (1997).
[14] D. G. Coronell, D. E. Hanson, A. F. Voter, C. L. Liu, and J. D. Kress, Appl. Phys. Lett. **73**, 3860 (1998).
[15] J. D. Kress, D. E. Hanson, A. F. Voter, C. L. Liu, X. Y. Liu, and D. G. Coronell (unpublished).
[16] U. Hansen, P. Vogl, and V. Fiorentini, Phys. Rev. B **59**, 7856 (1999).
[17] D. Frenkel and B. Smit, *Understanding Molecular Simulations: From Algorithms to Applications* (Academic Press, Boston, 1996).
[18] M. P. Allen and D. J. Tildesley, *Computer Simulation of Liquids* (Oxford University Press, Oxford, 1996).
[19] H. C. Huang, G. H. Gilmer, and T. D. de la Rubia, J. Appl. Phys. **84**, 3636 (1998).
[20] J. A. Sethian, *Level Set Methods and Fast Marching Methods* (Cambridge University Press, Cambridge, 1999).
[21] M. S. Daw and M. I. Baskes, Phys. Rev. B **29**, 6443 (1984).
[22] M. S. Daw and M. I. Baskes, Phys. Rev. Lett. **50**, 1285 (1983).
[23] A. A. Abrahamson, Phys. Rev. **178**, 178 (1969).
[24] U. Hansen, P. Vogl, and V. Fiorentini, Phys. Rev. B **60**, 5055 (1999).
[25] U. Hansen and A. Kersch, Phys. Rev. B **60**, 14 417 (1999).
[26] R. Stumpf and M. Scheffler, Phys. Rev. B **53**, 4958 (1996).
[27] For near normal incidence, the reflection probability is very low. So only in the high-energy regime could we collect a statistically significant number of reflection events for the averaging procedure. For that reason the curves for energies lower than 125 eV start at 30°.
[28] We restrict ourselves to length scales in the range of μm, whereas the typical wafer diameter is up to 300 mm. There are, of course, inhomogeneities over the wafer but those will be effective over lengths of cm not μm.
[29] S. Hamaguchi and S. M. Rossnagel, J. Vac. Sci. Technol. B **13**, 183 (1995).
[30] W. W. Mullins, Metall. Mater. Trans. A **26**, 1917 (1995).
[31] S. Osher and J. A. Sethian, J. Comput. Phys. **79**, 12 (1988).
[32] D. Adalsteinsson and J. A. Sethian, J. Comput. Phys. **120**, 128 (1995).
[33] Marker/string methods use a discrete parametrized version of the interface boundary. The position of the nodes is updated by determining front information about the normals and curvature form the node points. Within this approach it is extremely difficult to handle topological merging and significant instabilities in the front can develop.
[34] Cell-based methods divide the computational domain into a set of cells that contain ''volume fractions.'' The volume fraction represents the fraction of each cell containing the physical material. Advantages of such techniques include the ability to handle topological changes; however, the determination of geometric quantities such as normals can be inaccurate.
[35] Characteristic methods use ''ray-trace''-like techniques. These methods require the adaptive addition and/or removal of rays, which can cause instabilities and/or over-smoothing.
[36] M. Kratzer, R. P. Brinkmann, H. Schmidt, and G. Wachutka (unpublished).
[37] The Thompson distribution assumes the limiting case of a completely isotropic distribution. Its shape is independent of the angle of incidence and the emission as well as of the type and energy of the projectile (Ref. 41). The distribution of particles emitted from the sputter source can be written as $f(E,\theta)dEd\omega \propto [E/(E+E_B)^3]\cos(\theta)dEd\omega$ where θ is the off-normal angle, E the energy of the particle, and E_B is the surface binding energy of the material.
[38] W. D. Westwood, in *Microelctronic Materials and Processes*, edited by R. A. Levy (Kluwer, Dordrecht, 1989), p. 133.
[39] E. Dullini, Nucl. Instrum. Methods Phys. Res. B **2**, 610 (1984).
[40] G. Zhong and J. Hopwood, J. Vac. Sci. Technol. B **17**, 405 (1999).
[41] A. Goehlich and H. F. Döbele, Nucl. Instrum. Methods Phys. Res. B **115**, 489 (1996).